ISSN 0965-5425, Computational Mathematics and Mathematical Physics, 2015, Vol. 55, No. 6, pp. 1051–1067. © Pleiades Publishing, Ltd., 2015.
Original Russian Text © K.N. Volkov, A.G. Karpenko, 2015, published in Zhurnal Vychislitel'noi Matematiki i Matematicheskoi Fiziki, 2015, Vol. 55, No. 6, pp. 1058–1075.

Preconditioning of Gas Dynamics Equations in Compressible Gas Flow Computations at Low Mach Numbers

K. N. Volkov and A. G. Karpenko

Baltic State Technical University "Voenmekh," ul. Pervaya Krasnoormeiskaya 1, St. Petersburg, 190005 Russia
e-mail: dsci@mail.ru

Received July 24, 2013

Abstract—Features of the simulation of low-velocity inviscid and viscous compressible gas flows are considered, and a finite-volume discretization of gas dynamics equations at low Mach numbers on unstructured meshes is discussed. Preconditioning based on the use of physical variables is used to speed up the convergence of time marching to a steady state and to improve the accuracy of the steady-state solution. The structure of the preconditioning matrix and the diagonalization of the Jacobian of the preconditioned system of equations are discussed. The capabilities of this approach are demonstrated using model gasdynamic simulations in a wide range of Mach numbers.

DOI: 10.1134/S0965542515060135

Keywords: preconditioning, gas dynamics, unstructured mesh, finite-volume method, Euler and Navier–Stokes equations.

1. INTRODUCTION

Fluid flows are described by a system of equations consisting of the continuity equation, momentum equation, energy equation, and an equation of state (see [1]). The momentum equation has various forms in the inviscid and viscous models (Euler equations for inviscid flows and the Navier–Stokes equation for viscous flows). If necessary, the Euler and Navier–Stokes equations are supplemented with turbulence model equations, chemical kinetics equations, and other relations.

Widely used for integrating the incompressible flow equations are the artificial compressibility (pseudo- compressibility) method [2], in which the time derivative of pressure is introduced into the continuity equation; the projection method [3], which is based on splitting over physical processes; and pressure projection methods [4]. A common feature of pressure projection methods is that the difference scheme is formulated in terms of increments of unknown functions and Poisson's equation is solved for the pressure correction term at every time step. In the case of implicit difference schemes, widely applied are the alternating direction implicit (ADI) method [5], relaxation-type methods [6], the lower-upper symmetric Gauss–Seidel (LU-SGS) method [7], and others. An overview and comparison of various approaches can be found in [8].

Numerical methods for compressible gas equations that perform well at moderately subsonic and supersonic flow velocities become low effective or unsuitable as applied to flows at low Mach numbers ($M < 0.2$) [1], which is manifested by slower convergence of time marching to a steady state and by the loss of accuracy of the resulting steady-state solutions (see [9–12]). The slower convergence of time marching is explained by the fact that the stiffness of the compressible Euler and Navier–Stokes equations increases as $M \longrightarrow 0$ (this feature is exhibited at the differential level). The stiffness is characterized by the ratio of the maximum to minimum eigenvalues of the Jacobian (the ratio of the maximum to minimum propagation velocities of perturbations). The integration time step is determined by the velocity of the fastest wave (acoustic waves, $\lambda = |u + c|$), while the time required for reaching a steady state depends on the velocity of the slowest wave (convective waves, $\lambda = |u|$). In viscous problems and turbulent flow computations on stretched grids in boundary layers, the time step is restricted by the acoustic solution modes and by the mesh size in the normal direction to the wall [13, 14].

The numerical simulation of flows at low Mach numbers is based on the incompressible Euler or Navier–Stokes equations with the use of suitable methods. For $M < 0.3$, the incompressible fluid model provides a fairly accurate approximation with an error of about 5%. The full Euler or Navier–Stokes equations are required for simulating high-velocity flows with extended low-velocity subregions [15] (e.g., flows with deceleration and recirculation zones for internal flows in diffusers with a subsonic inlet velocity)

and low-velocity flows with density and temperature variations caused by heat supply (for example, free convective flows).

The transition to the limit form (as $M \longrightarrow 0$) of the Navier–Stokes equations for hyposonic nonisothermal viscous gas flows makes it possible to partially eliminate the difficulties arising in computing these flows relying on the full Navier–Stokes equations (see [16]).

A popular method for eliminating the computational difficulties arising as $M \longrightarrow 0$ is related to various techniques of preconditioning the original equations, which are aimed at leveling the orders of the eigenvalues of the Jacobian for all $M < 1$ (see [17–23]). At the differential level, preconditioning modifies the terms involving time derivatives in the momentum equations. In a steady state, the solution of the modified (preconditioned) system coincides with that of the original system of equations. An unsteady solution is found by applying dual time-stepping [24].

Preconditioning is also widely used to accelerate the convergence of iterative methods as applied to systems of difference equations generated by finite-difference or finite-volume discretizations of the Euler and Navier–Stokes equations (stiffness is exhibited in matrices).

Preconditioning makes it possible to eliminate the stiffness of the original system and to accelerate the convergence of time marching to a steady state [9–12]. Additionally, subsonic flows can be computed more accurately by applying a modified discretization of convective fluxes in the preconditioned equations [25, 26]. In the general case, preconditioning changes the form of the underlying equations and the properties of difference schemes because it introduces artificial viscosity. Additionally, it raises questions concerning the applicability of boundary conditions. The accuracy of preconditioned difference schemes degrades with increasing Mach number. Theoretical issues related to the preconditioning of the Euler and Navier–Stokes equations at low Mach numbers are discussed in [8, 20, 27, 28], while various preconditioning approaches are compared in [29].

Widely used in practice are the methods developed in [9–11, 17–19]. The application domain of the method from [9–11] is restricted to central-difference schemes, which perform well at $M < 1$, but become dissipative in supersonic flow simulation. The method of [17–19] can fairly easily be applied to upwind difference schemes and has been widely used in external gasdynamic simulations (see [13, 14]). The local preconditioning of the Euler and Navier–Stokes equations was applied in [30, 31]. In this case, the transition to modified equations depends on the local Mach number (external flows) or the local pressure field (internal flows). In many cases, preconditioning methods are combined with other convergence acceleration methods [15], such as residual smoothing and multigrid methods.

While numerical computations are usually based on equations written in conservative variables, the preconditioning matrix is constructed using physical variables, which simplify the construction procedure [20]. Entropy (symmetrized variables) is used as a dependent variable in [20], while temperature (physical variables) is applied for this purpose in [9–11, 16]. A preconditioning matrix that modifies only the energy equation is used in [9, 10]. A method intended for simulating viscous flows is presented in [11]. The preconditioning procedure in [32] is designed so as to optimize the propagation velocities of waves in the entire range of Mach numbers (optimal condition number).

In this paper, for the Euler and Navier–Stokes equations, we develop a preconditioning method that makes it possible to construct a universal numerical procedure for computing inviscid and viscous compressible gas flows in a wide range of Mach numbers (from essentially subsonic to transonic and supersonic flow velocities). The preconditioning matrix is constructed by applying the approach proposed in [16], which was implemented in the one-dimensional case in [1]. This approach relies on physical variables (one of which is temperature). Its features include a specific form of writing fluxes, the computation of a dissipative term in the course of finding the fluxes through control volume faces, and a specific representation of matrices in the diagonalization of the inviscid flux Jacobian of the preconditioned system. The dissipative term in the difference scheme for flux computation is written in a compact form. The capabilities of the approach are demonstrated by solving several model problems in internal gas dynamics.

2. COMPUTATIONS AT LOW MACH NUMBERS

Consider the linearized Euler equations

$$\frac{\partial U}{\partial t} + A\frac{\partial U}{\partial x} = 0,$$

where $A = \partial F/\partial U$ is the Jacobian. The eigenvalues of the Jacobian are $\lambda_1 = u$, $\lambda_2 = u - c$, and $\lambda_3 = u + c$. The condition number of the matrix A has the form

$$k(A) = \varrho(A)\varrho(A^{-1}),$$

where ϱ is the spectral radius. For $k \gg 1$, the matrix A is ill-conditioned, which causes difficulties in solving the corresponding system of difference equations.

Assuming for simplicity that $u > 0$, we represent the condition number as

$$k(A) = (u + c)\max\left\{\frac{1}{u}, \frac{1}{|u - c|}\right\} = \max\left\{1 + \frac{1}{\mathrm{M}}, \frac{\mathrm{M} + 1}{|\mathrm{M} - 1|}\right\}.$$

The Jacobian is ill-conditioned at the sonic point (as $\mathrm{M} \longrightarrow 1$) and in low Mach number flows (as $\mathrm{M} \longrightarrow 0$).

The computational difficulties near the sonic point can be overcome by adding dissipative terms (see [33]).

For the explicit Euler scheme, the stability condition has the form $\Delta t \le \Delta x/(u + c)$. In subsonic flows, the physical time step is on the order of the characteristic time scale $\Delta\tau = \Delta x/u$. Comparing the numerical and physical time steps, we obtain

$$\frac{\Delta t}{\Delta\tau} \le \frac{\mathrm{M}}{1 + \mathrm{M}}.$$

At low Mach numbers, the numerical time step is less than the physical one and the system of gas dynamics equations is stiff.

3. FINITE-VOLUME METHOD

In conservative variables, the equation describing an unsteady viscous compressible gas flow is written as

$$\frac{\partial U}{\partial t} + \nabla \cdot [F(U) + G(U, \nabla U)] = 0, \tag{1}$$

where U is the vector of conservative variables, $F(U)$ is the vector of inviscid fluxes, and $G(U, \nabla U)$ is the vector of viscous fluxes. For simplicity, the source term in Eq. (1) is omitted.

Integrating Eq. (1) over the control volume (CV) V with boundary ∂V, whose orientation is specified by the outer unit normal $\mathbf{n}$, and applying the Gauss–Ostrogradsky theorem, we obtain

$$\frac{\partial}{\partial t}\int\limits_V U d\Omega + \int\limits_{\partial V} F(U)\cdot\mathbf{n} dS + \int\limits_{\partial V} G(U)\cdot\mathbf{n} dS = 0. \tag{2}$$

The Navier–Stokes equations written in the form of (2) are spatially discretized using the vertex-centered finite-volume method on an unstructured mesh. The explicit Euler method or the explicit two-step Runge–Kutta method is used for time differencing. Inviscid fluxes are discretized by applying the Roe scheme, while viscous fluxes are discretized with the help of a second-order accurate centered scheme. Some details of the implementation of the finite-volume method are discussed in [15, 31].

4. PRECONDITIONING MATRIX

At low Mach numbers, the flow is described by an equation written in physical variables. The new set of physical variables is defined as

$$Q = \begin{pmatrix} p \\ v_x \\ v_y \\ v_z \\ T \end{pmatrix}.$$

For incompressible flows, the velocity and temperature gradients are required for computing viscous flows and the pressure gradient is needed for solution interpolation. In the computations, we use the excess pres-

sure $p - p^*$, which is taken into account when the density is found from the equation of state (in the basic equations, the pressure is under the integral sign).

The equations describing the flow at low Mach numbers are written in physical variables:

$$\Gamma \frac{\partial}{\partial t} \int\limits_{V_i} Q dV + \int\limits_{\partial V_i} F dS = 0. \tag{3}$$

The preconditioning matrix is represented as

$$\Gamma = \begin{pmatrix} \Theta & 0 & 0 & 0 & \rho_T \\ \Theta v_x & \rho & 0 & 0 & \rho_T v_x \\ \Theta v_y & 0 & \rho & 0 & \rho_T v_y \\ \Theta v_z & 0 & 0 & \rho & \rho_T v_z \\ \Theta H - 1 & \rho v_x & \rho v_y & \rho v_z & \rho_T H + \rho c_p \end{pmatrix},$$

where $H = c_p T + |\mathbf{v}|^2/2$ (here, c_p is the specific heat capacity at constant pressure). The density derivatives with respect to pressure at constant temperature and with respect to temperature at constant pressure are determined by the relations

$$\rho_p = \left.\frac{\partial \rho}{\partial p}\right|_T, \quad \rho_T = \left.\frac{\partial \rho}{\partial T}\right|_p.$$

The parameter Θ is given by

$$\Theta = \left(\frac{1}{U_r^2} - \frac{\rho_T}{\rho c_p}\right),$$

where U_r is the propagation velocity of pressure perturbations.

For an ideal gas, $\rho_p = 1/(RT) = \gamma/c^2$, where c is the speed of sound, while, for constant-density flows, we have $\rho_p = 0$, which leads to pressure perturbations propagating at an infinite velocity in an incompressible fluid. To eliminate the singularity, ρ_p is assumed to be inversely proportional to the local velocity squared (the propagation velocity of pressure perturbations is equal to the local velocity). As a result, the eigenvalues of the Jacobian become of the same order and the Euler and Navier–Stokes equations at low Mach numbers are no longer stiff.

For an ideal gas, the parameter U_r is defined as

$$U_r = \begin{cases} \varepsilon c, & |\mathbf{v}| < \varepsilon c, \\ |\mathbf{v}|, & \varepsilon c < |\mathbf{v}| < c, \\ c, & |\mathbf{v}| > c. \end{cases}$$

The preconditioning mechanism is used when the local velocity of the flow is less than the speed of sound (then $U_r = u$). In a supersonic flow region, preconditioning is not used ($U_r = c$) and preconditioned system (3) passes into system (2) for compressible gas flows. For $u \ll c$ (for example, at stagnation points), U_r is bounded by a certain value.

For incompressible and variable-density fluids (for example, when the Boussinesq approximation is used for free convective flows), the parameter U_r is specified as

$$U_r = \begin{cases} \varepsilon U_{\max}, & |\mathbf{v}| < \varepsilon U_{\max}, \\ |\mathbf{v}|, & |\mathbf{v}| > \varepsilon U_{\max}, \end{cases}$$

where $U_{\max}$ is the maximum flow velocity.

To represent viscous fluxes correctly, it is necessary that the propagation velocity of acoustic perturbations associated with the eigenvalues of the modified system of equations be no less than the propagation velocity of viscous perturbations (see [16]). A switch is introduced in CVs where the velocity is so low that the eigenvalues of the preconditioned system become less than the propagation velocity of viscous pertur-

bations (for example, in boundary and mixing layers, where viscous effects are dominant). The parameter U_r is replaced by

$$U_r^* = \max\left\{U_r, \frac{\mu}{\rho\Delta x}\right\}.$$

The eigenvalues of the Jacobian of the preconditioned system are found by solving the characteristic equation $|A - \lambda\Gamma| = 0$, where $A = \partial F_x/\partial Q$. As a result, we obtain

$$\lambda_{1,2,3} = v_x, \quad \lambda_{4,5} = v_x' \mp c',$$

where

$$v_x' = v_x(1-\alpha), \quad c' = (\alpha^2 v_x^2 + U_r^2)^{1/2}.$$

The parameter α is given by the relation

$$\alpha = \frac{1}{2}(1 - \beta U_r^2), \quad \beta = \rho_p + \frac{\rho_T}{\rho c_p}.$$

In supersonic flows, $U_r = c$, $\alpha = 0$, and the eigenvalues are of the same order and equal to the eigenvalues of the original system ($\lambda_{1,2,3} = v_x$, $\lambda_{4,5} = v_x \mp c$). At low Mach numbers ($|v_x| \ll c$), we obtain $\alpha \longrightarrow 1/2$ as $U_r \longrightarrow 0$ and the eigenvalues have the same order and tend to the value

$$v_x' \mp c' = \frac{1}{2}v_x(1 \mp \sqrt{5}).$$

In the case of incompressible flows, $\beta = 0$ and $\alpha = 1/2$ (there is no dependence on U_r), the eigenvalues are also of the same order, and the stiffness of the system is eliminated as $M \longrightarrow 0$.

5. FEATURES OF THE DISCRETIZATION

A finite-volume discretization of Eq. (3) yields

$$\Gamma\frac{dQ_i}{dt} + \frac{1}{V_i}\sum_j^{N_i}(F_{ij} + G_{ij})S_{ij} = 0. \tag{4}$$

The inviscid fluxes on a CV face are determined using the relation

$$F_{i+1/2} = \frac{1}{2}(F_R + F_L) - \frac{1}{2}|A|_{i+1/2}\Delta U.$$

The viscous fluxes G_{ij} are computed in the same manner as without preconditioning (see [15]). The second order in space is achieved by interpolating the gradients to a CV face.

The shortcomings of the numerical algorithms as $M \longrightarrow 0$ are eliminated by preconditioning the dissipative term of the difference scheme (see [17]). The dissipative term is represented as

$$|A|\Delta U = \Gamma\Gamma^{-1}\frac{\partial F_x}{\partial U}\Delta U = \Gamma\left(\Gamma^{-1}\frac{\partial F_x}{\partial U}\right)\Delta Q = \Gamma|A_\Gamma|\Delta Q,$$

where $A_\Gamma = \Gamma^{-1}(\partial F_X/\partial Q)$. The eigenvalues λ_4 and λ_5 are corrected near the sonic point [33]. In contrast to the Roe scheme, the arithmetic means of parameter values are used to compute the eigenvalues and coefficients of the matrices A_Γ and Γ.

Diagonalizing the Jacobian matrix $A_\Gamma = M_\Gamma\Lambda_\Gamma M_\Gamma^{-1}$ of the preconditioned system, we write the difference scheme in the form

$$F_{i+1/2} = \frac{1}{2}(F_R + F_L) - \frac{1}{2}\Gamma M_\Gamma|\Lambda_\Gamma|M_\Gamma^{-1}\Delta Q.$$

For explicit difference schemes, the dissipative term simplifies to

$$|A_\Gamma|\Delta Q = M_\Gamma|\Lambda_\Gamma|M_\Gamma^{-1}\Delta Q = \begin{pmatrix} c^*\Delta p + M^*(\rho U_r^2\Delta v_x - \alpha v_x\Delta p) \\ c^*\Delta v_x + M^*(\alpha v_x\Delta v_x + \Delta dp/\rho) \\ |\lambda_1|\Delta v_y \\ |\lambda_1|\Delta v_z \\ [c^*\Delta p + M^*(\rho U_r^2\Delta v_x - \alpha v_x\Delta p) + |\lambda_1|(\rho c_p\Delta T - \Delta p)]/(\rho c_p) \end{pmatrix},$$

where

$$M^* = \frac{1}{2c'}(|\lambda_5| + |\lambda_4|), \quad c^* = \frac{1}{2}(|\lambda_5| + |\lambda_4|).$$

Here, Δp, Δv_x, Δv_y, Δv_z, and ΔT denote the jumps in pressure, velocity, and temperature on the CV face, respectively. The eigenvalues of the Jacobian are given by $\lambda_1 = v_x$, $\lambda_4 = u' - c'$, and $\lambda_5 = u' + c'$.

The order of accuracy in space is increased by applying an approach based on linear distributions of the parameters over a CV. The variables at the center of the CV Q_i are interpolated to a face:

$$Q'_L = Q_L + (\nabla Q)_L|\Delta\mathbf{r}_L|, \quad Q'_R = Q_R + (\nabla Q)_R|\Delta\mathbf{r}_R|,$$

where ∇Q is the gradient at the CV center and $\Delta\mathbf{r}_L$ and $\Delta\mathbf{r}_R$ are the vectors directed from the centers of neighboring CVs L and R to the midpoint of the separating face.

6. TIME MARCHING TO A STEADY STATE

Equation (4) is written in semidiscrete form:

$$\frac{dQ_i}{dt} = -\Gamma^{-1}R. \tag{5}$$

Discretizing the residual yields

$$R = \frac{1}{V_i}\sum_j^{N_i} F_{ij}S_{ij}.$$

The time differencing of Eq. (5) is based on the explicit Euler method. Specifically, at the time level $n + 1$, the variables are determined using the relations

$$Q_i^{n+1} = Q_i^n + \Delta t\Gamma^{-1}(Q_i^n)R(Q^n).$$

At use of the explicit two-step Runge–Kutta method for a discretization of Eq. (5) in time variables on a layer $n + 1$ in time are from relations

$$Q_i^* = Q_i^n + \Delta t\Gamma^{-1}(Q_i^n)R(Q^n),$$

$$Q_i^{n+1} = Q_i^n + \Delta t\Gamma^{-1}(Q_i^*)R(Q^*).$$

When stationary problems are solved by applying time marching, the time derivative in Eq. (5) vanishes as $t \longrightarrow \infty$. Accordingly, the solution of Eq. (5) is regarded as the solution to the original system of equations. The time step is chosen as based on the highest propagation velocity of pseudopressure perturbations or viscous perturbations and is calculated using the formula

$$\Delta t = \min\left\{\mathrm{CFL}\frac{\Delta x}{|u'| + c'}, \sigma\frac{\rho\Delta x^2}{\mu}\right\},$$

where CFL is the Courant number, σ is a parameter bounding the time step in the case of viscous problems, and Δx is the shortest distance from the CV center to the face.

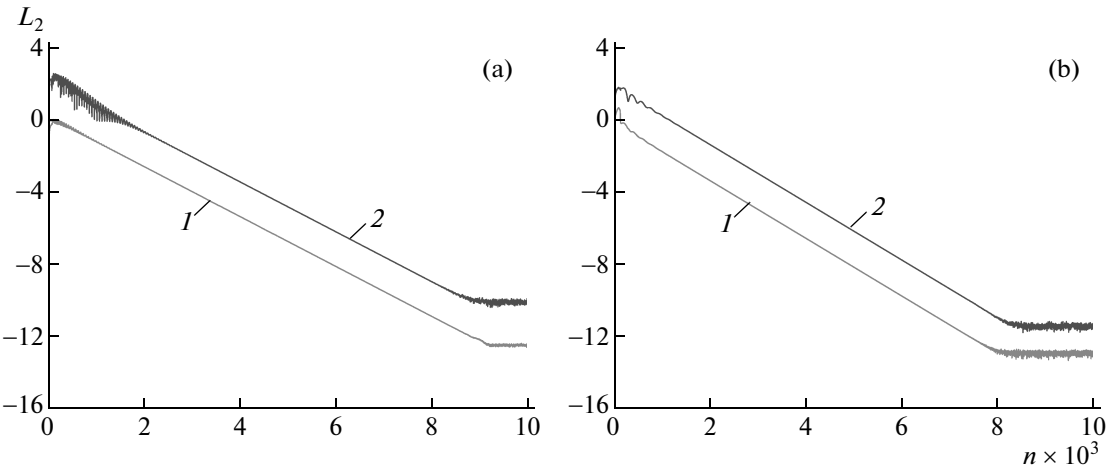

Fig. 1. Convergence rate of the solutions of the (a) original and (b) preconditioned equations at $\Delta p = 1600$ Pa.

7. NUMERICAL RESULTS

A series of model gasdynamic simulations in a wide range of Mach numbers were used to analyze the convergence rate and accuracy of steady-state solutions of the original and preconditioned gas dynamics equations. These equations were integrated until a steady-state solution was reached. As a convergence criterion, we used the residual norm

$$L_2(U) = \left[\sum_{i=1}^{N} (U_i^{n+1} - U_i^n)^2\right]^{1/2}.$$

The numerical solution was said to converge if $L_2 \le \varepsilon$, where ε is a small prescribed quantity ($\varepsilon \sim 10^{-16}$ was used in the computations).

7.1. Nozzle Flow

Consider the inviscid compressible gas flow in a channel with a variable cross-sectional area. The nozzle profile is described by the relation

$$y = \left(\frac{1+x^2}{\pi}\right)^{1/2},$$

where $x \in [-0.3, 1]$.

The flow regime in the nozzle is determined by the relation between the reservoir pressure p_1 and the exit pressure p_2 ($\Delta p = p_1 - p_2$ was specified in the computations). In version 1 (the pressure drop is less than a critical value), the flow has a shock wave sitting at the exit. In version 2 (the pressure drop is greater than the critical value) the gas steadily accelerates from subsonic inlet conditions to a speed in the critical cross section that depends on the specified pressure drop and then decelerates. The computations were performed on a grid of 100 cells at CFL = 0.95.

In version 1 we specify the stagnation pressure ($p_1 = 10^6$ Pa) and the stagnation temperature ($T_1 = 300$ K) in the inlet cross section, while the static pressure ($p_2 = 8 \times 10^5$ Pa) is set in the exit cross section. The flow at the inlet of the computational domain is subsonic. In the converging section of the nozzle, the gas accelerates, reaches the speed of sound in the critical cross section, and moves further at a supersonic speed. In the expanding section of the nozzle, there develops a normal shock wave, behind which the flow becomes subsonic. With the given parameters, we have $M > 0.4$ in the entire computational domain, so the solutions of the original and preconditioned equations coincide.

In version 2 the gas accelerates in the subsonic section and decelerates in the supersonic one. Figures 1–4 show the convergence rates of the time marching procedure in the form of the residual norm as a function of the number of time steps for the original and preconditioned equations. Lines (*1*) and (*2*) depict the residuals caused by discretizing the momentum and pressure equations, respectively.

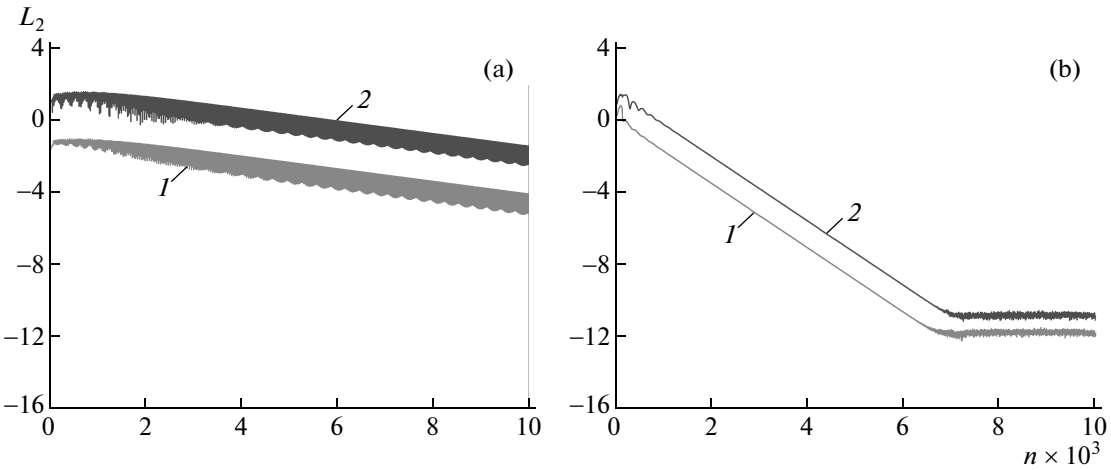

Fig. 2. Convergence rate of the solutions of the (a) original and (b) preconditioned equations at $\Delta p = 175$ Pa.

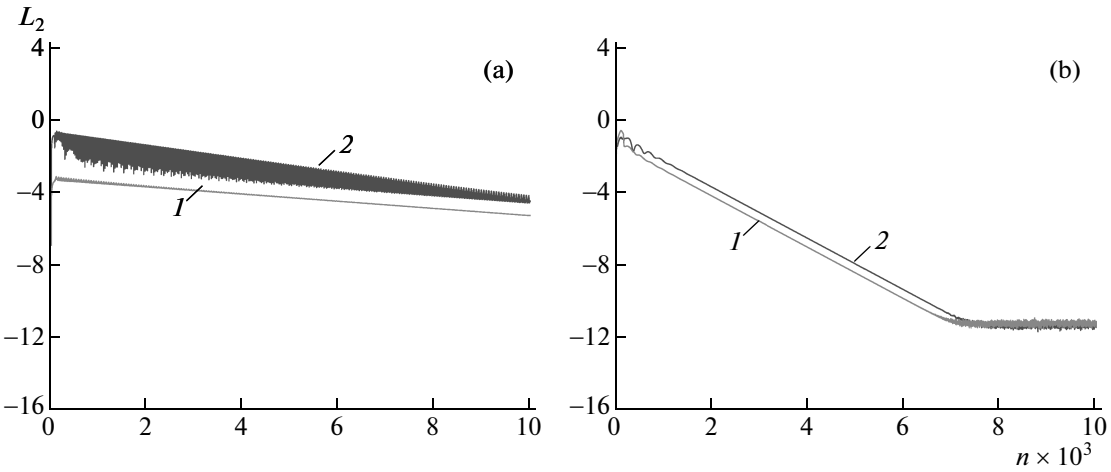

Fig. 3. Convergence rate of the solutions of the (a) original and (b) preconditioned equations at $\Delta p = 1.8$ Pa.

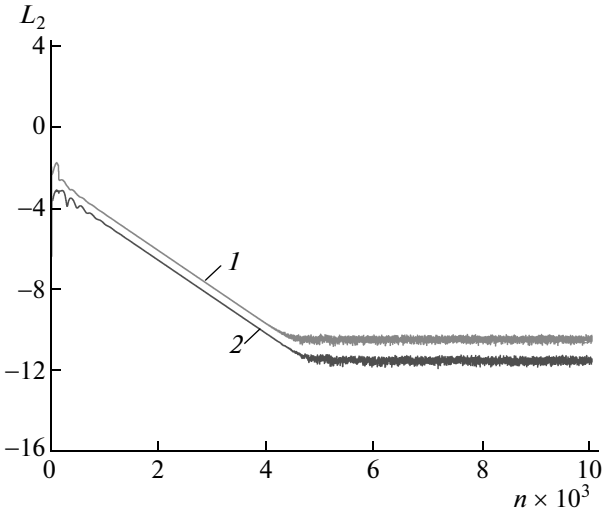

Fig. 4. Convergence rate of the solution of the preconditioned equations at $\Delta p = 0.02$ Pa.

At $\Delta p = 1600$ Pa, the Mach number in the critical cross section is approximately M = 0.3. The convergence of the numerical solution is shown in Fig. 1. The flow velocity remains sufficiently high in the entire computational domain, so the solutions based on two numerical procedures nearly coincide. The residual patterns are also similar in both cases. However, the solution of the original equations exhibits a lower residual (Fig. 1a) than that of the preconditioned equations (Fig. 1b). The solution produced by time marching reaches a steady state after about 9×10^3 time steps in the case of the original equations and after 8×10^3 time steps in the case of preconditioning.

When the pressure drop is reduced to $\Delta p = 175$ Pa, the Mach number in the critical cross section becomes M = 0.1. The convergence of the numerical solution is shown in Fig. 2. The solutions of the original and preconditioned Euler equations are now different. Due to the developed preconditioning approach, the prescribed residual level is achieved after about 7×10^3 time steps (Fig. 2b). For the original equations, the convergence rate of the time marching procedure is rather slow and the prescribed residual level is not achieved after 10^4 time steps (Fig. 2a).

As the pressure drop is decreases still further to $\Delta p = 1.8$ Pa, the Mach number in the critical cross section becomes M = 0.01. The convergence of the numerical solution is shown in Fig. 3. The Mach number distributions along the nozzle axis differ substantially in the case of the original and preconditioned equations (the distributions of flow characteristics are not shown). Due to the preconditioning procedure, the convergence pattern becomes nearly independent of the pressure drop (Fig. 3b), while the convergence of the solution to the original equations degrades (Fig. 3a).

When the pressure drop is reduced to $\Delta p = 0.02$ Pa, the Mach number in the critical cross section is M = 0.001. The solution of the original equations becomes divergent. The convergence of the solution of the preconditioned equations is illustrated in Fig. 4. The prescribed residual is achieved after 4.8×10^3 time steps.

The variation in the residual shown in Fig. 4 is similar to the convergence patterns presented in Figs. 2 and 3, which suggests that the time marching procedure depends weakly on the Mach number in the computational domain. Relying on the approach developed, we can compute the characteristics of the nozzle flow from essentially subsonic to supersonic velocities.

7.2. Flow through a Channel with a Bump

Consider the flow through a plane channel with a bump. The length-to-height ratio in the channel is $L/H = 4$, and the maximum height of the bump (which is a circular arc) is $0.1H$ (the maximum bump is 10% of the channel width). The computations were performed on a grid of 120×20 cells (Fig. 5) with 60 nodes placed on the bump surface.

Flows through a channel with a bump were computed, for example, in [9, 34]. Specifically, the implicit Euler time differencing and the Beam–Warming scheme for discretizing inviscid fluxes were used in [9]. The computations in [34] were based on Godunov's method and were performed in a wide range of Mach numbers.

The velocity ($U = 3.47$ m/s), pressure ($p = 10^5$ Pa), and temperature ($T = 300$ K) were set in the inlet cross section of the channel, while mild boundary conditions (free outflow) were specified in the outlet cross section. The inlet cross section conditions corresponded to M = 0.01. A steady-state solution of the problem was obtained by taking 5000 time steps of the time marching procedure.

Figure 6 displays level lines of the velocity magnitude. In contrast to the solution of the original equations, a velocity distribution symmetric about the vertical axis is obtained in the case of preconditioning.

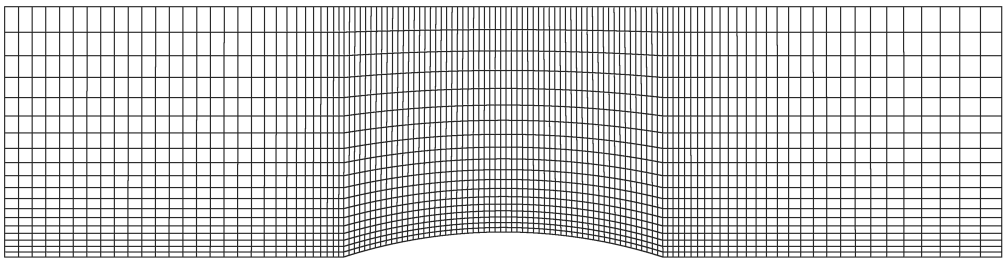

Fig. 5. Numerical grid.

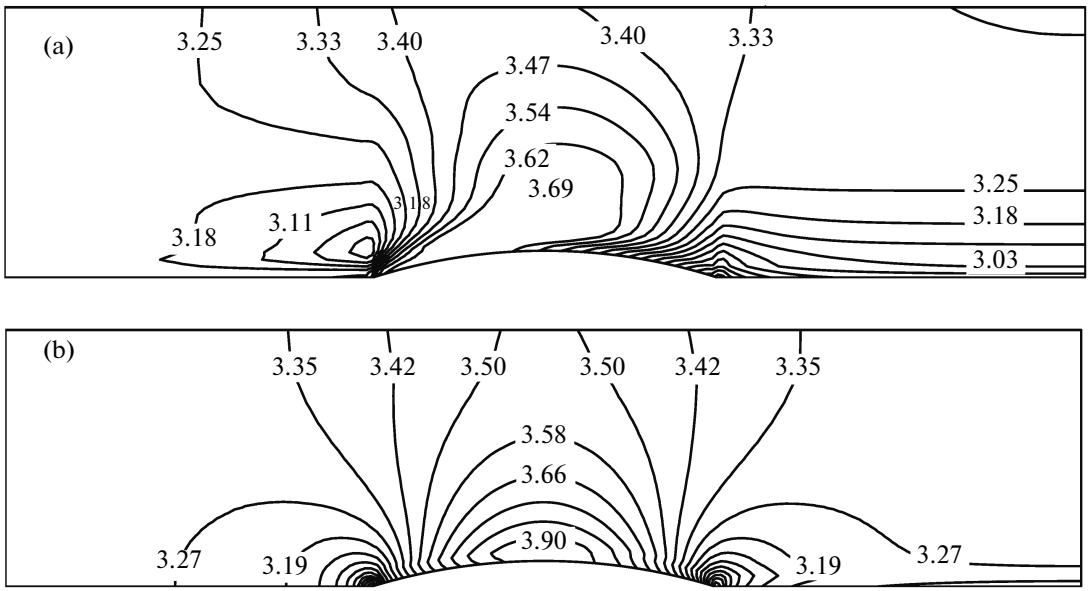

Fig. 6. Level lines of the velocity magnitude in the case of the (a) original and (b) preconditioned equations.

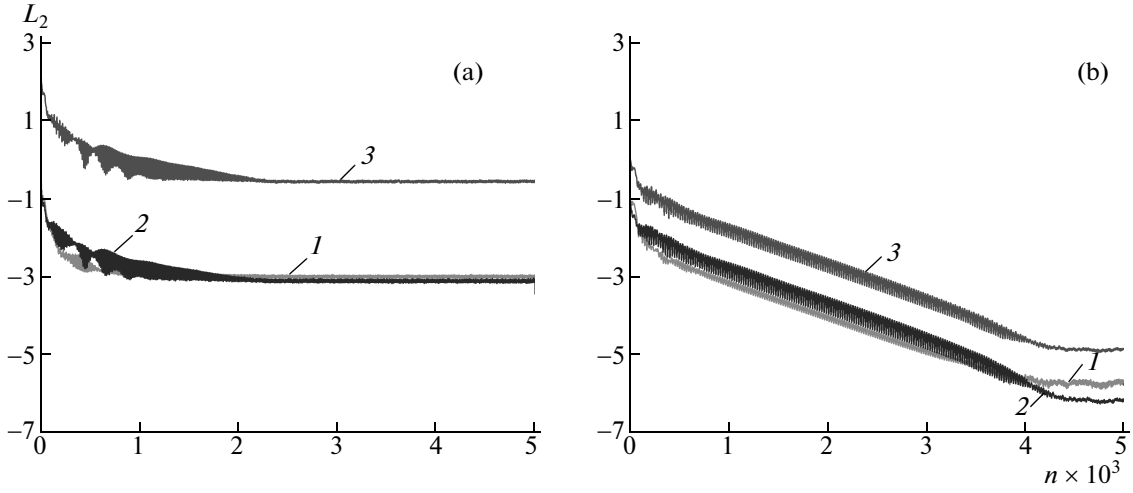

Fig. 7. Convergence rate of the solutions of the (a) original and (b) preconditioned equations.

The convergence rate of the time marching procedure is shown in Fig. 7. The original equations were solved in conservative variables, while the preconditioned equations were computed in physical variables. Curves (*1*) and (*2*) depict the residuals (in physical variables) caused by discretizing the momentum equation, while curve (*3*) shows the residual caused by discretizing the pressure equation. In the case of preconditioning, the prescribed residual is obtained after about 3500 iteration steps. For the original equations, the residuals with respect to velocity and pressure are two orders of magnitude higher and the convergence rate nearly ceases to vary after 4000 time steps.

To test the performance and accuracy of the numerical method in a wide range of Mach numbers, the computations were performed in subsonic, transonic, and supersonic regimes. More specifically, the flow was computed in a channel with a 10% bump (as in the underlying version) on a grid of 144×32 cells at $M = 0.5$ (subsonic) and $M = 0.675$ (transonic) and in a channel with a 4% bump on a grid of 220×60 cells at $M = 1.65$ (supersonic).

For subsonic and supersonic regimes, Fig. 8 shows level lines of the velocity magnitude at various inlet Mach numbers. For relatively low inlet Mach numbers, the flow is nearly symmetric about the vertical axis

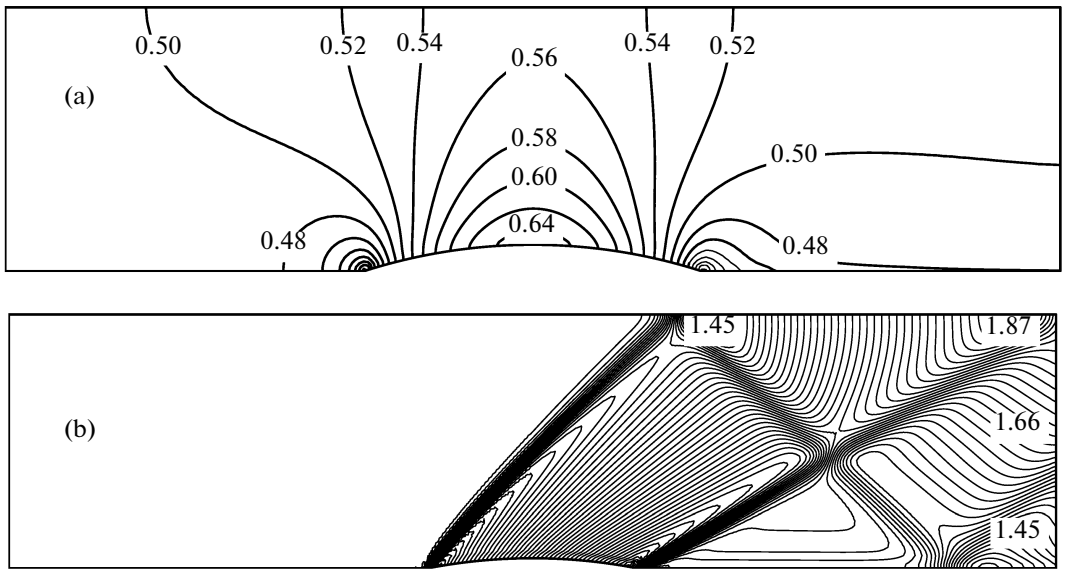

Fig. 8. Level lines of the velocity magnitude at (a) M = 0.5 and (b) M = 1.65.

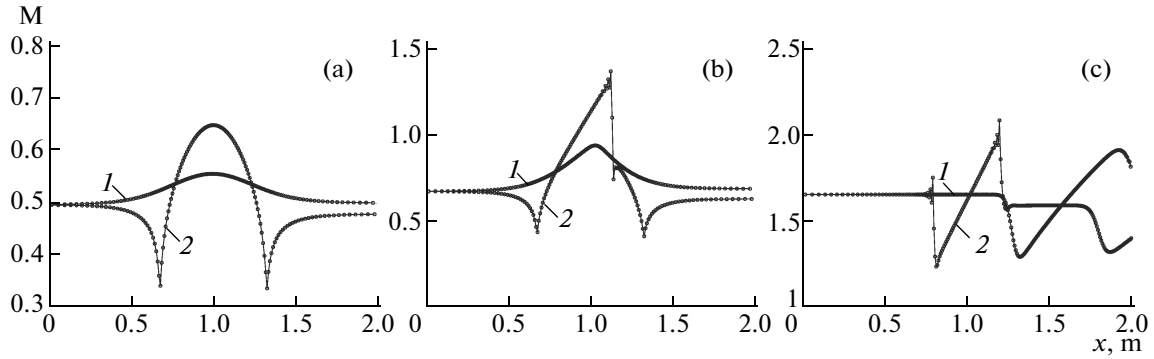

Fig. 9. Mach number distribution along the (*1*) upper and (*2*) lower channel walls at (a) M = 0.5, (b) M = 0.675, and (c) M = 1.65.

(Fig. 8a). The weak asymmetry of the flow is associated with the leading and trailing edges of the bump (a horseshoe vortex of weak intensity develops behind the bump). To eliminate these shortcomings, the flow characteristics near the corner points are computed by interpolating the flow parameters from interior nodes of the computational domain (see [34]). At high inlet Mach numbers, shock waves develop and interact in the flow (Fig. 8b). The inclination angles of the shocks and the level lines agree well with the numerical data presented in [34].

Figure 9 presents the Mach number distributions on the upper (curve *1*) and lower (curve *2*) walls of the channel in various flow regimes. These distributions agree well with numerical data from [34] (as in the case of velocity magnitude level lines, weak differences are observed on the lower wall of the channel near the corner points).

8. CONCLUSIONS

A numerical method was developed for computing steady inviscid and viscous compressible gas in a wide range of Mach numbers. The accuracy and convergence rate of the method are independent of the Mach number. The original and preconditioned equations are discretized by applying the finite-volume method on an unstructured mesh. An explicit scheme is used for time differencing, while the inviscid and viscous fluxes are discretized with the help of second-order accurate schemes. Preconditioning is switched

on depending on the local Mach number or the local pressure field (specifically, the preconditioned equations are always solved for the incompressible fluid model).

The numerical results obtained in the test problems suggest that the numerical method developed has a sufficient accuracy for resolving characteristic features of incompressible and compressed flows. Due to the preconditioning procedure, the convergence rate of time marching is made independent of the Mach number. At low Mach numbers, the CPU time required for solving the preconditioned equations is more by about 15% (due to an increase in the number of arithmetic operations) than in the case of the original equations.

The finite-volume method was implemented on general-purpose graphics processing units, which makes the explicit schemes competitive with implicit numerical methods.

APPENDIX

Below are the auxiliary relations required for computing preconditioning matrix.

Physical and Conservative Variables

In integral form, the system of gas dynamics equations describing unsteady viscous compressible gas flows has the form

$$\frac{\partial}{\partial t}\int\limits_{V_i} U dV + \int\limits_{\partial V_i} (F+G)dS = 0.$$

In physical variables, it becomes

$$\frac{\partial U}{\partial Q}\frac{\partial}{\partial t}\int\limits_{V_i} Q dV + \int\limits_{\partial V_i} (F+G)dS = 0.$$

The vectors of physical and conservative variables are given by

$$Q = \begin{pmatrix} p \\ v_x \\ v_y \\ v_z \\ T \end{pmatrix}, \quad U = \begin{pmatrix} \rho \\ \rho v_x \\ \rho v_y \\ \rho v_z \\ \rho e \end{pmatrix},$$

respectively. The transition between the conservative and physical variables is based on the matrix

$$\frac{\partial U}{\partial Q} = \begin{pmatrix} \rho_p & 0 & 0 & 0 & \rho_T \\ \rho_p v_x & \rho & 0 & 0 & \rho_T v_x \\ \rho_p v_y & 0 & \rho & 0 & \rho_T v_y \\ \rho_p v_z & 0 & 0 & \rho & \rho_T v_z \\ \rho_p H - 1 & \rho v_x & \rho v_y & \rho v_z & \rho_T H + \rho c_p \end{pmatrix}.$$

Construction of the Preconditioning Matrix

Multiplying the equation written in physical variables by a matrix K, we obtain the following equation in nonconservative form:

$$\left(K\frac{\partial U}{\partial Q}\right)\frac{\partial}{\partial t}\int\limits_{V_i} Q dV + K\int\limits_{\partial V_i} F dS = 0.$$

The matrix K is chosen so as to simplify the product

$$K\frac{\partial U}{\partial Q} = \begin{pmatrix} \rho_p & 0 & 0 & 0 & \rho_T \\ 0 & \rho & 0 & 0 & 0 \\ 0 & 0 & \rho & 0 & 0 \\ 0 & 0 & 0 & \rho & 0 \\ -1 & 0 & 0 & 0 & \rho c_p \end{pmatrix}.$$

It has the form

$$K = \begin{pmatrix} 1 & 0 & 0 & 0 & 0 \\ -v_x & 1 & 0 & 0 & 0 \\ -v_y & 0 & 1 & 0 & 0 \\ -v_z & 0 & 0 & 1 & 0 \\ -(H-|\mathbf{v}|^2) & -v_x & -v_y & -v_z & 1 \end{pmatrix}.$$

The modified matrix $\tilde{\Gamma} = K(\partial U/\partial Q)$ for the system of nonconservative equations is given by

$$\tilde{\Gamma} = \begin{pmatrix} \Theta & 0 & 0 & 0 & \rho_T \\ 0 & \rho & 0 & 0 & 0 \\ 0 & 0 & \rho & 0 & 0 \\ 0 & 0 & 0 & \rho & 0 \\ -1 & 0 & 0 & 0 & \rho c_p \end{pmatrix}.$$

Multiplying the equation by the matrix K^{-1}, we pass to the conservative preconditioned equation

$$\Gamma\frac{\partial}{\partial t}\int\limits_{V_i} Q dV + K\int\limits_{\partial V_i} F dS = 0,$$

where $\Gamma = K^{-1}\tilde{\Gamma}$. The inverse of the matrix Γ has the form

$$\Gamma^{-1} = \begin{pmatrix} ab + U_r^2 & a v_x & a v_y & a v_z & a \\ -v_x/\rho & 1/\rho & 0 & 0 & 0 \\ -v_y/\rho & 0 & 1/\rho & 0 & 0 \\ -v_z/\rho & 0 & 0 & 1/\rho & 0 \\ [b(a-1)+U_r^2]/(\rho c_p) & e v_x & e v_y & e v_z & -e \end{pmatrix},$$

where $a = \rho_T U_r^2/(\rho c_p)$, $b = H - |\mathbf{v}|^2$, and $e = (a-1)/(\rho c_p)$.

The eigenvalues of the Jacobian of the preconditioned system are found by solving the characteristic equation

$$\left|\Gamma^{-1}A - \lambda I\right| = |A - \lambda\Gamma| = 0,$$

where $A = \partial F_x/\partial Q$. The flux Jacobian in physical variables has the form

$$A = \begin{pmatrix} \rho_p v_x & \rho & 0 & 0 & \rho_T v_x \\ \rho_p v_x^2 + 1 & 2\rho v_x & 0 & 0 & \rho_T v_x^2 \\ \rho_p v_x v_y & \rho v_y & \rho v_x & 0 & \rho_T v_x v_y \\ \rho_p v_x v_z & \rho v_z & 0 & \rho v_x & \rho_T v_x v_z \\ \rho_p H v_x & \rho(H + v_x^2) & \rho v_x v_y & \rho v_x v_z & (\rho_T H + \rho c_p) v_x \end{pmatrix}.$$

Rearranging the determinant, we obtain

$$\begin{vmatrix} \rho_p v_x - \lambda\Theta & \rho & 0 & 0 & \rho_T(v_x - \lambda) \\ 1 & \rho(v_x - \lambda) & 0 & 0 & 0 \\ 1 & 0 & \rho(v_x - \lambda) & 0 & 0 \\ 1 & 0 & 0 & \rho(v_x - \lambda) & 0 \\ \lambda & \rho v_x(v_x - \lambda) & \rho v_y(v_x - \lambda) & \rho v_z(v_x - \lambda) & \rho c_p(v_x - \lambda) \end{vmatrix} = 0.$$

The characteristic equation becomes

$$(v_x - \lambda)^3[\rho c_p - v_x^2(\rho_T + \rho\rho_p c_p) + \lambda v_x(2\rho_T + \rho\rho_p c_p + \Theta\rho c_p) - \lambda^2(\rho_T + \Theta\rho c_p)] = 0.$$

We have $\Lambda_{1,2,3} = v_x$, while the roots $\lambda_{4,5}$ are found by solving the quadratic equation

$$\lambda^2 - v_x(1 + \beta U_r^2)\lambda - U_r^2(1 - \beta v_x^2) = 0,$$

where $\beta = \rho_p + \rho_T/(\rho c_p)$. For the ideal gas model, $\beta = 1/(\gamma RT) = 1/c^2$. Solving the quadratic equation yields

$$\lambda_{4,5} = v_x' \mp c',$$

where

$$v_x' = v_x(1 - \alpha), \quad c' = (\alpha^2 v_x^2 + U_r^2)^{1/2}.$$

The parameter α is given by the relation

$$\alpha = \frac{1}{2}(1 - \beta U_r^2).$$

Eigenvalues and Eigenvectors

The right eigenvectors of the matrix A_Γ are determined by the relation $A_\Gamma \mathbf{r}_i = \lambda_i \mathbf{r}_i$, which gives

$$(A - \lambda_i\Gamma)\mathbf{r}_i = 0.$$

After substitution and simple transformations, we obtain

$$\begin{pmatrix} \rho_p v_x - \lambda\Theta & \rho & 0 & 0 & \rho_T(v_x - \lambda) \\ 1 & \rho(v_x - \lambda) & 0 & 0 & 0 \\ 1 & 0 & \rho(v_x - \lambda) & 0 & 0 \\ 1 & 0 & 0 & \rho(v_x - \lambda) & 0 \\ \lambda & \rho v_x(v_x - \lambda) & \rho v_y(v_x - \lambda) & \rho v_z(v_x - \lambda) & \rho c_p(v_x - \lambda) \end{pmatrix} \begin{pmatrix} r_1 \\ r_2 \\ r_3 \\ r_4 \\ r_5 \end{pmatrix} = 0.$$

At $\lambda = v_x$, the equation becomes

$$\begin{pmatrix} \rho_p v_x - v_x\Theta & \rho & 0 & 0 & 0 \\ 1 & 0 & 0 & 0 & 0 \\ 1 & 0 & 0 & 0 & 0 \\ 1 & 0 & 0 & 0 & 0 \\ \lambda & 0 & 0 & 0 & 0 \end{pmatrix} \begin{pmatrix} r_1 \\ r_2 \\ r_3 \\ r_4 \\ r_5 \end{pmatrix} = 0.$$

Here, $r_1 = 0$ and $r_2 = 0$, while the components r_3, r_4, and r_5 are chosen to be linearly independent:

$$\mathbf{r}_1 = \begin{pmatrix} 0 \\ 0 \\ 0 \\ 0 \\ 1 \end{pmatrix}, \quad \mathbf{r}_2 = \begin{pmatrix} 0 \\ 0 \\ 0 \\ 1 \\ 0 \end{pmatrix}, \quad \mathbf{r}_3 = \begin{pmatrix} 0 \\ 0 \\ 1 \\ 0 \\ 0 \end{pmatrix}.$$

For the components of the right eigenvectors $\mathbf{r}_4$ and $\mathbf{r}_5$ with eigenvalues $\lambda_4 = v_x' - c'$ and $\lambda_5 = v_x' + c'$, we obtain

$$r_2 = \frac{r_1}{\rho(\lambda - v_x)}, \quad r_3 = 0, \quad r_4 = 0, \quad r_5 = \frac{r_1}{\rho c_p}.$$

Since $\lambda = u' - c'$, we have $\lambda - u = -(\alpha u + c')$ and $r_1 = \alpha u + c'$. The eigenvector corresponding to the eigenvalue λ_4 is given by

$$\mathbf{r}_4 = \begin{pmatrix} \alpha u + c' \\ -1/\rho \\ 0 \\ 0 \\ (\alpha u + c')/(\rho c_p) \end{pmatrix}.$$

For the eigenvalue $\lambda_5 = u' + c'$, we obtain $\lambda - u = -(\alpha u - c')$. Setting $r_1 = \alpha u - c'$ yields

$$\mathbf{r}_5 = \begin{pmatrix} \alpha u - c' \\ -1/\rho \\ 0 \\ 0 \\ (\alpha u - c')/(\rho c_p) \end{pmatrix}.$$

The right eigenvector matrix is written as

$$M_\Gamma = \begin{pmatrix} 0 & 0 & 0 & (\alpha u + c') & (\alpha u - c') \\ 0 & 0 & 0 & -1/\rho & -1/\rho \\ 0 & 0 & 1 & 0 & 0 \\ 0 & 1 & 0 & 0 & 0 \\ 1 & 0 & 0 & (\alpha u + c')/(\rho c_p) & (\alpha u - c')/(\rho c_p) \end{pmatrix}.$$

The left eigenvector matrix (the inverse of M_Γ) has the form

$$M_\Gamma^{-1} = \begin{pmatrix} -1/(\rho c_p) & 0 & 0\ 0\ 1 \\ 0 & 0 & 0\ 1\ 0 \\ 0 & 0 & 1\ 0\ 0 \\ 1/(2c') & \rho(\alpha u - c')/(2c') & 0\ 0\ 0 \\ -1/(2c') & -\rho(\alpha u + c')/(2c') & 0\ 0\ 0 \end{pmatrix}.$$

The eigenvalue matrix Λ is given by

$$\Lambda = \begin{pmatrix} v_x & 0 & 0 & 0 & 0 \\ 0 & v_x & 0 & 0 & 0 \\ 0 & 0 & v_x & 0 & 0 \\ 0 & 0 & 0 & u - (\alpha u + c') & 0 \\ 0 & 0 & 0 & 0 & u - (\alpha u - c') \end{pmatrix}.$$

The matrix $A_\Gamma = \Gamma^{-1}A$ is written as

$$A_\Gamma = \begin{pmatrix} v_x\beta U_r^2 & \rho U_r^2 & 0 & 0 & 0 \\ 1/\rho & v_x & 0 & 0 & 0 \\ 0 & 0 & v_x & 0 & 0 \\ 0 & 0 & 0 & v_x & 0 \\ -2\alpha v_x/(\rho c_p) & U_r^2/c_p & 0 & 0 & v_x \end{pmatrix}.$$

REFERENCES

1. P. Wesseling, *Principles of Computational Fluid Dynamics* (Springer, New York, 2000).
2. A. J. Chorin, "A numerical method for solving incompressible viscous flow problems," J. Comput. Phys. **2** (1), 12–26 (1967).
3. A. J. Chorin, "Numerical solution of the Navier–Stokes Equations," Math. Comput. **22** (104), 745–762 (1968).
4. S. V. Patankar and D. B. Spalding, "A calculation procedure for heat, mass and momentum transfer in three-dimensional parabolic flows," Int. J. Heat Mass Transfer **15** (10), 1787–1806 (1972).
5. W. R. Briley and H. McDonald, "Solution of the multidimensional compressible Navier–Stokes equations by a generalized implicit method," J. Comput. Phys. **24** (4), 372–397 (1977).
6. R. W. MacCormack, "Current status of numerical solutions of the Navier–Stokes equations," AIAA Paper, No. 85-0032 (1985).
7. S. Yoon and D. Kwak, "LU-SGS implicit algorithm for three-dimensional incompressible Navier–Stokes equations with source term," AIAA Paper, No. 89-1964 (1989).
8. D. Kwak, C. Kiris, and J. Housman, "Implicit methods for viscous incompressible flows," Comput. Fluids **41** (1), 51–64 (2011).
9. D. Choi and C. L. Merkle, "Application of time-iterative schemes to incompressible flow," AIAA J. **23** (10), 1518–1524 (1985).
10. C. L. Merkle and Y.-H. Choi, "Computation of low-speed compressible flows with time marching procedures," Int. J. Numer. Methods Eng. **25** (2), 293–311 (1988).
11. Y.-H. Choi and C. L. Merkle, "The application of preconditioning in viscous flows," J. Comput. Phys. **105** (2), 207–223 (1993).
12. G. Volpe, "Performance of compressible flow codes at low Mach numbers," AIAA J. **31** (1), 49–56 (1993).
13. N. A. Pierce and M. B. Giles, "Preconditioning Compressible flow calculations on stretched meshes," AIAA Paper, No. 96-0889 (1996).
14. N. A. Pierce and M. B. Giles, "Preconditioned multigrid method for compressible flow calculations on stretched meshes," J. Comput. Phys. **136** (2), 425–445 (1997).

15. K. N. Volkov and V. N. Emel'yanov, *Numerical Techniques in Computational Fluid Dynamics* (Fizmatlit, Moscow, 2012) [in Russian].
16. J. M. Weiss and W. A. Smith, "Preconditioning applied to variable and constant density flows," AIAA J. **33** (11), 2050–2057 (1995).
17. E. Turkel, A. Fiterman, and B. Van Leer, "Preconditioning and the limit to the incompressible flow equations," ICASE Report, No. 93-42 (1993).
18. E. Turkel, V. Vatsa, and R. Radespiel, "Preconditioning methods for low-speed flows," AIAA Paper, No. 96-2640 (1996).
19. E. Turkel, "Preconditioning-squared methods for multidimensional aerodynamics," AIAA Paper, No. 97-2025 (1997).
20. E. Turkel, R. Radespiel, and N. Kroll, "Assessment of preconditioning methods for multidimensional aerodynamics," Comput. Fluids **26** (6), 613–634 (1997).
21. D. L. Darmofal and P. J. Schmid, "The importance of eigenvectors for local preconditioning of the Euler equations," J. Comput. Phys. **127** (2), 346–362 (1996).
22. H. Guillard and C. Viozat, "On the behavior of the upwind schemes in the low Mach number limit," Comput. Fluids **28** (1), 63–86 (1999).
23. J. M. Weiss, J. P. Maruszewski, and W. A. Smith, "Implicit solution of preconditioned Navier–Stokes equations using algebraic multigrid," AIAA J. **37** (1), 29–36 (1999).
24. S.-H. Lee, "Cancellation problem of preconditioning method at low Mach numbers," J. Comput. Phys. **225** (2), 1199–1210 (2007).
25. J.-S. Shuen, K.-H. Chen, and Y. Choi, "A coupled implicit method for chemical non-equilibrium flows at all speeds," J. Comput. Phys. **106** (2), 306–318 (1993).
26. J. Housman, C. Kiris, and M. Hafez, "Preconditioned methods for simulations of low speed compressible flows," Comput. Fluids **38** (7), 1411–1423 (2009).
27. S. Venkateswaran and C. L. Merkle, "Analysis of preconditioning methods for the Euler and Navier–Stokes equations," *Von Karman Institute Lecture Series on CFD*, No. 1999-30 (1999).
28. D. L. Darmofal, P. Moinier, and M. B. Giles, "Eigenmode analysis of boundary conditions for the one-dimensional preconditioned Euler equations," J. Comput. Phys. **160** (1), 369–384 (2000).
29. Y. Colin, H. Deniau, and J.-F. Boussuge, "A robust low speed preconditioning formulation: Application to air intake flows," Comput. Fluids **47** (1), 1–15 (2011).
30. P. Moinier and M. B. Giles, "Compressible Navier–Stokes equations for low Mach number applications," *Proceedings of the ECCOMAS Computational Fluid Dynamics Conference, September 4–7, 2001* (Swansea, UK, 2001).
31. K. N. Volkov, "Preconditioning of the Euler and Navier–Stokes equations in low-velocity flow simulation on unstructured grids," Comput. Math. Math. Phys. **49** (10), 1789–1804 (2009).
32. W. Lee and P. Roe, "Characteristic time-stepping or local preconditioning of the Euler equations," AIAA Paper, No. 91-1552 (1991).
33. A. Harten, "High resolution schemes for hyperbolic conservation laws," J. Comput. Phys. **49** (3), 357–393 (1983).
34. S. Eidelman, P. Colella, and R. P. Shreeve, "Application of the Godunov method and its second-order extension to cascade flow modeling," AIAA J. **22** (11), 1609–1615 (1984).

Translated by I. Ruzanova

SPELL: OK